Nuclear-localized subtype of end-binding 1 protein regulates spindle organization in *Arabidopsis*

Shinichiro Komaki[1], Tatsuya Abe[1], Silvie Coutuer[2,3], Dirk Inzé[2,3], Eugenia Russinova[2,3] and Takashi Hashimoto[1,*]

[1]Graduate School of Biological Sciences, Nara Institute of Science and Technology, Ikoma, Nara 630-0192, Japan
[2]Department of Plant Systems Biology, Flanders Institute for Biotechnology, B-9052 Gent, Belgium
[3]Department of Plant Biotechnology and Genetics, Ghent University, B-9052 Gent, Belgium
*Author for correspondence (hasimoto@bs.naist.jp)

Summary

End-binding 1 (EB1) proteins are evolutionarily conserved plus-end-tracking proteins that localize to growing microtubule plus ends where they regulate microtubule dynamics and interactions with intracellular targets. Animal EB1 proteins have acidic C-terminal tails that might induce an autoinhibitory conformation. Although EB1 proteins with the same structural features occur in plants (EB1a and EB1b in *Arabidopsis thaliana*), a variant form (EB1c) is present that lacks the characteristic tail. We show that in *Arabidopsis* the tail region of EB1b, but not of EB1c, inhibits microtubule assembly in vitro. EB1a and EB1b form heterodimers with each other, but not with EB1c. Furthermore, the *EB1* genes are expressed in various cell types of *Arabidopsis*, but the expression of *EB1c* is particularly strong in the meristematic cells where it is targeted to the nucleus by a nuclear localization signal in the C-terminal tail. Reduced expression of *EB1c* compromised the alignment of spindle and phragmoplast microtubules and caused frequent lagging of separating chromosomes at anaphase. Roots of the *eb1c* mutant were hypersensitive to a microtubule-disrupting drug and complete rescue of the mutant phenotype required the tail region of EB1c. These results suggest that a plant-specific EB1 subtype has evolved to function preferentially on the spindle microtubules by accumulating in the prophase nucleus.

Key words: *Arabidopsis thaliana*, EB1, Microtubule, Nuclear localization, Spindle

Introduction

Microtubules (MTs) are dynamic polar polymers that establish cell shape, facilitate cell motility, organize organelles, and assist with cell division. The more dynamic plus end with fast-growing and shortening characteristics plays an important role by providing binding sites for regulatory proteins, designated plus end-tracking proteins (+TIPs) (Akhmanova and Steinmetz, 2008). Among them, the family of end-binding 1 (EB1) proteins appear to be the main integrators of protein complexes assembled at the plus end because animal EB1 proteins and the yeast homologs Mal3p and Bim1p specifically track the growing MT ends independently of their binding partners in a cell-free system (Bieling et al., 2008; Bieling et al., 2007; Komarova et al., 2009; Zimniak et al., 2009). Mouse EB1 and Mal3p promote the assembly of MTs with 13 protofilaments; this number being found almost universally in vivo (des Georges et al., 2008; Vitre et al., 2008). EB1 regulates the behavior of the plus ends, either directly or by recruiting other +TIPs (Akhmanova and Steinmetz, 2008). Depletion of EB1 in a number of cell systems results in nondynamic MTs that spend most of the time in a paused state (Tirnauer and Bierer, 2000). In mitotic metazoan cells, EB1 is targeted to the kinetochores to which polymerizing MT ends are attached (Tirnauer et al., 2002) and is required for proper dynamics of spindle MTs and for chromosome segregation (Draviam et al., 2006; Green et al., 2005).

The EB protein family contains an N-terminal calponin homology (CH) domain and a composite C-terminal (CC) domain consisting of an α-helically coiled coil partially overlapping with a unique EB1 homology region (Fig. 1A). The C-terminal tail of 20-30 residues is rich in acidic residues and generally ends with a conserved acidic-aromatic C-terminus, designated the EEY/F motif

(Akhmanova and Steinmetz, 2008). Studies on yeast and metazoan EB1 proteins demonstrated that the CH domain is necessary and sufficient for MT binding (Bu and Su, 2003; Komarova et al., 2009), whereas the CC domain mediates the parallel dimerization of EB1 monomers and provides a binding surface for EB1-interacting proteins (Slep et al., 2005). The EEY/F motif at the flexible tail region provides a binding site for CAP-Gly domains found in select cytoskeleton-associated proteins, including a +TIP p150[Glued] (Honnappa et al., 2009; Steinmetz and Akhmanova, 2008). Deletion of the EEY/F motif from EB1 abolishes the formation of the EB1-p150[glued] complex and strongly increases the ability of EB1 to assemble MTs and to suppress shortening dynamics in vitro (Hayashi et al., 2005; Manna et al., 2008). In this attractive model, the C-terminal tail interacts normally with the N-terminal CH domain and inhibits its MT-binding capacity, which is relieved by binding of p150[glued] or other +TIPs to the EEY/F motif (Hayashi et al., 2005). Whether this model is applicable to EB1 proteins of various organisms and their interacting partners is still unknown.

EB1 homologs are also found in plant lineages (Bisgrove et al., 2004; Guo et al., 2009), but interestingly, the EEY/F motif is not present in plant EB1 proteins, which are divided in two subgroups. In *Arabidopsis thaliana*, EB1a and EB1b represent one subgroup that possesses an acidic tail region reminiscent to the yeast and metazoan EB1 proteins, whereas EB1c constitutes another subgroup that contains a tail region with patches of basic amino acid residues (supplementary material Fig. S1). Green fluorescent proteins (GFPs) fused to EB1a or EB1b have been shown to track growing plus ends of MTs in plant cells (Chan et al., 2003; Dixit et al., 2006; Mathur et al., 2003). Although the plus-end tracking of EB1c has not been demonstrated, EB1c-GFP accumulated in the interphase

nucleus (Dixit et al., 2006) and an EB1c-enriched pool of antibodies was found to label the midzone region of spindles and phragmoplasts where the plus ends of MTs are more concentrated (Bisgrove et al., 2008). T-DNA insertion mutants with highly reduced expression of the *Arabidopsis EB1* genes gave surprisingly mild phenotypes; *eb1b* mutant roots grew towards the left on vertically placed agar plates, indicative of mild defects on organization of cortical MT arrays (Ishida et al. 2007), while that of *eb1c* mutant roots was hypersensitive to a MT-disrupting drug (Bisgrove et al., 2008).

Here, we show that the functions for the CH and CC domains are conserved in the *Arabidopsis* EB1 proteins. Furthermore, the C-terminal tail of the EB1a and EB1b subgroup is autoinhibitory in the MT assembly capacity of EB1, despite the absence of the EEY/F motif; instead, the EB1c tail has a nuclear localization signal (NLS). Our cell biological and complementation results indicate that by its unique C-terminal tail EB1c functions preferentially at the early stages of plant mitosis by regulating spindle positioning and chromosome segregation.

Results

Characterization of functional domains of *Arabidopsis* EB1 proteins

Arabidopsis contains three EB1 proteins: EB1a and EB1b, with most closely related amino acid sequences, and EB1c. We defined the MT-binding region by testing fragments of recombinant EB1 proteins in a sedimentation assay with Taxol-stabilized MTs (Fig. 1A; supplementary material Fig. S2). Full-length EB1a, EB1b and EB1c, and the EB1b and EB1c fragments lacking the C-terminal tail regions (ΔTs) pelleted with polymerized MTs, whereas the CH domains alone and the fragments lacking the CH domains (ΔCHs) were recovered in the supernatant fractions. Addition of the linker region to the CH domain (CH-L) in EB1b and EB1c resulted in partial sedimentation with the polymer, in line with yeast and human EB1 proteins in which the linker region enhances the plus-end tracking activity of the CH domain (des Georges et al., 2008; Komarova et al., 2009; Zimniak et al., 2009).

Full-length EB1b (and EB1a; data not shown) interacted with each other in a yeast two-hybrid assay (Fig. 1B). The simultaneous substitution of alanine for Y217 and I224 in the CC domain abolished the homodimeric interaction. These two conserved residues are required for dimerization of the human EB1 (Slep et al., 2005). Gel filtration experiments showed that the recombinant EB1b fragment without the CH domain formed a dimer, but that the Y217-I224 mutant eluted at a monomer position (Fig. 1C). These results indicate that the CH-L and CC domains of the *Arabidopsis* EB1 proteins mediate MT binding and dimerization, respectively, as demonstrated for non-plant EB1 proteins (Akhmanova and Steinmetz, 2008).

Heterodimerization between *Arabidopsis* EB1 proteins was analyzed by a pull-down assay (Fig. 1D). Since mammalian EB dimers readily exchange their subunits in vitro (Komarova et al., 2009), we tested whether full-length *Arabidopsis* His-tagged EB1 proteins exchange their subunits with nontagged EB1 fragments during a 5-minute incubation at 37°C. Nontagged fragments of EB1a and EB1b associated with the full-length His-tagged EB1a and EB1b, but not with that of EB1c. Conversely, nontagged EB1c interacted with tagged EB1c, but not with tagged EB1a or EB1b. Therefore, EB1a and EB1b form heterodimers with each other, but not with EB1c in vitro.

To examine the functional roles of the C-terminal tail on tubulin polymerization, we carried out a turbidity assay in the presence of
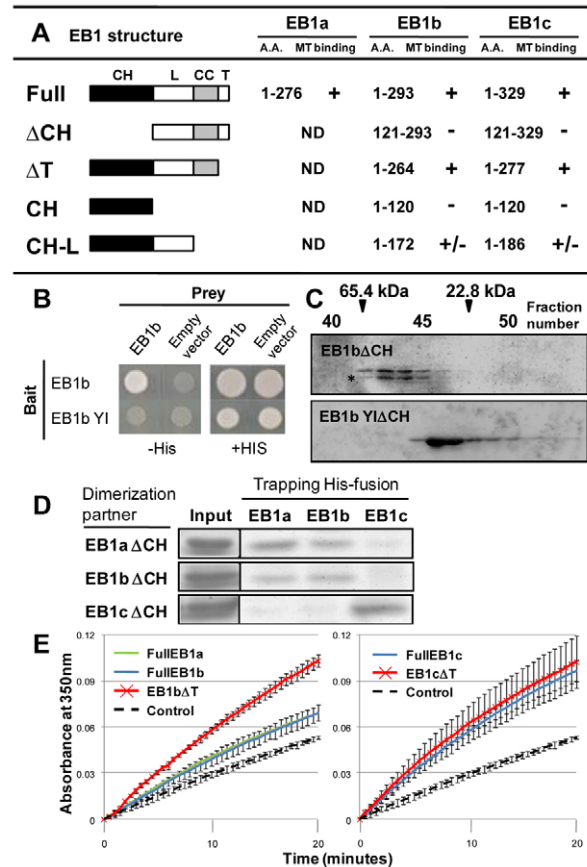

Fig. 1. Characterization of *Arabidopsis* EB1 domains in vitro. (**A**) Schematic summary of the mapping of the MT-binding domain of EB1b and EB1c. Plus and minus symbols indicate that proteins did and did not bind MTs, respectively. CH, calponin-homologous domain; L, linker region; CC, coiled-coil EB1 homology domain; T, tail region; A.A., amino acids; N.D., not determined. (**B**) Yeast two-hybrid assay. Wild-type EB1b interacted with itself to form a homodimer, but did not associate with a YI mutant of EB1b. The growth medium of the plates in the left panel lacked histidine to select for interacting combinations. (**C**) Gel filtration assay. EB1b fragments lacking the CH domain were eluted from a gel filtration column and analyzed by 12.5% SDS-PAGE and staining with Coomassie brilliant blue. An asterisk indicates the position of a probable degradation product of EB1b ΔCH. (**D**) Dimerization between EB1 proteins. After EB1 ΔCH fragments had been incubated individually with a full-length 6×His-tagged protein, the formed dimer was retained on an affinity column, eluted, analyzed by SDS-PAGE, and stained with Coomassie brilliant blue. (**E**) Autoinhibition of MT assembly by C-terminal tail regions of EB1. The kinetics of tubulin polymerization was measured by the increase in sample absorption at 350 nm. In the left graph, much stronger polymerization-promoting activity was observed for EB1bΔT (red) than for full-length EB1a (green) and EB1b (blue). Control indicates spontaneous MT assembly in the absence of EB1 proteins. By contrast, the right graph shows strong tubulin polymerization by both full-length EB1c and EB1cΔT.

nucleating MT seeds. Full-length EB1a and EB1b increased the optical turbidity of the tubulin solution (Fig. 1E). Notably, the *eb1b* mutant without an acidic tail (EB1ΔT) assembled MTs more efficiently than the full-length protein. By contrast, the full-length EB1c strongly promoted tubulin polymerization, whereas the activity did not further increase by deletion of its C-terminal tail. These results suggest that the acidic tail region of EB1b inhibits the MT assembly, possibly by interacting with the N-terminal MT-binding CH domain. However, the EB1c tail had no such autoinhibitory function.
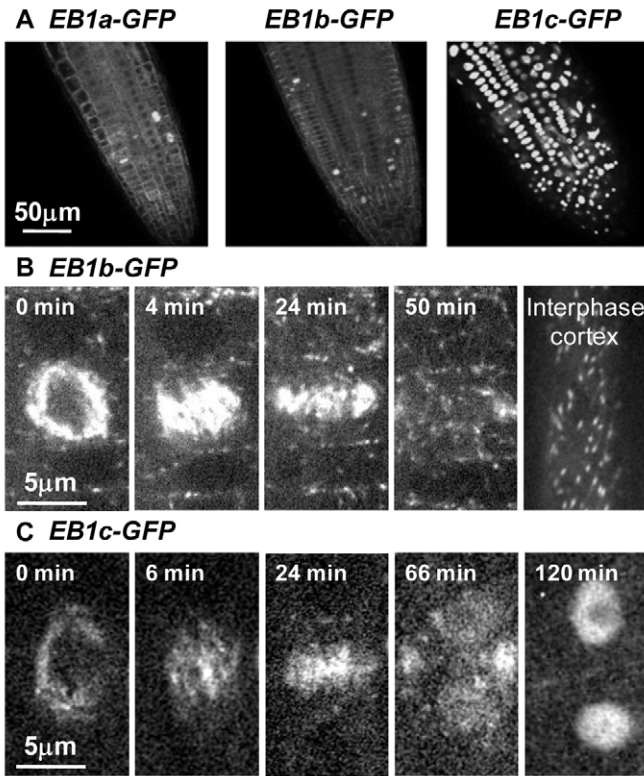
Fig. 2. Expression patterns and subcellular localization of EB1 proteins. EB1-GFP fusion proteins were produced under their native regulatory elements in *Arabidopsis*. (**A**) Labeling of mitotic MTs by all three EB1-GFP proteins in the root meristematic regions. (**B**) Distribution of EB1b-GFP during the cell cycle progression. Comet-like dots indicate growing plus ends of the endoplasmic or cortical MTs. The panel on the right shows the cortical region in an interphase cell. The distribution of EB1a-GFP was very similar (data not shown). The time of the nuclear envelope breakdown was set at 0 minutes. (**C**) Distribution of EB1c-GFP during the cell cycle progression.

Fig. 3. The tail region of EB1c possesses a functional NLS. GFP fusion proteins were transiently produced in onion epidermal cells. (**A**) Amino acid sequences of the C-terminal EB1 tail regions in *Arabidopsis*, tobacco and rice (*Oryza sativa*). Plant EB1 proteins can be classified in two subfamilies, based on the presence or absence of two basic motifs (Box1 and Box2) in their tail regions. Acidic and basic amino acids are shown in red and green, respectively. Mutations introduced into Box1 (*m1*) and Box2 (*m2*) are indicated. (**B**) Subcellular localization and MT association of various EB1 mutants analyzed as chimeric proteins to the C-terminus of GFP or GFP-GUS. (**C**) Examples of transient expression assays of GFP fusion proteins in onion cells. Dotted lines in the upper panel indicate the cell contour.

Expression patterns and subcellular localization

To analyze the expression patterns of *EB1* genes and the localization of EB1 proteins, we inserted GFP just in front of the stop codons of the genomic fragments, encompassing the >2-kb 5′-upstream regions and >1-kb 3′-downstream regions. These *EB1-GFP* constructs were introduced into wild-type and *eb1* mutant *Arabidopsis* plants. As the *EB1c-GFP* construct efficiently complemented the *eb1c* mutant phenotype (see below), it was fully functional. All *EB1* genes were expressed in various tissue types, but relatively strongly in the guard cells of leaf stomata and in the pollen tube (supplementary material Fig. S3). The expression of *EB1c* was particularly prominent in the shoot and root meristems (Fig. 2A and supplementary material Fig. S3). These expression patterns were consistent with the tissue-specific gene expression data of Genevestigator (Zimmermann et al., 2004) and with our own quantitative RT-PCR results (supplementary material Fig. S4).

At the root meristem, all three *EB1-GFP* constructs decorated mitotic MT structures (Fig. 2A). Time-lapse microscopy was used to follow the distribution of GFP fusion proteins during the cell cycle. EB1a-GFP (data not shown) and EB1b-GFP stained the growing plus end of interphase and mitotic MTs (Fig. 2B; supplementary material Movie 1). After the apparent disintegration of the nuclear envelope, EB1c-GFP decorated peripheral spindle
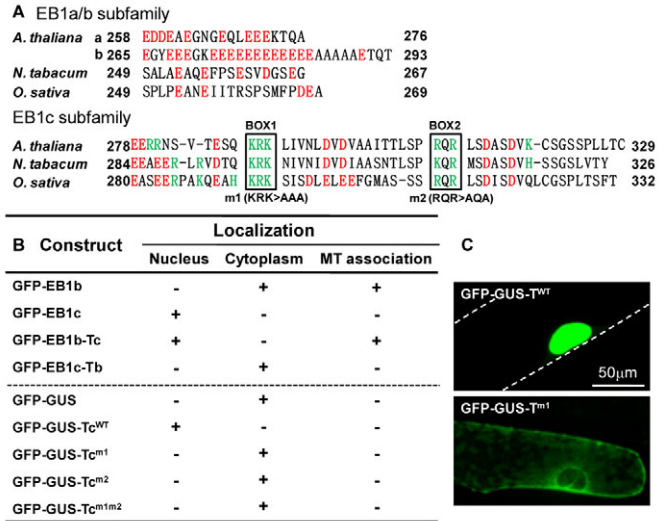
MTs that were located near the former nuclear envelope and then labeled whole spindles within a few minutes (Fig. 2C; supplementary material Movie 2). After EB1c-GFP-labeled phragmoplasts matured (66 minutes), EB1c-GFP began to accumulate in the nucleus. At this stage, EB1c-GFP also labeled endoplasmic and cortical MTs at their plus ends (supplementary material Movie 3, and see later). Eventually, all visible GFP signals were located in the nucleus (120 minutes), indicating active recruitment of EB1c into the nucleus.

The EB1c tail contains a functional NLS

To study the structural determinants for differential subcellular distributions of the *Arabidopsis* EB1 proteins, we focused on their divergent C-terminal regions (Fig. 3A). Wild-type EB1b, wild-type EB1c, and chimeric EB1 proteins in which the tail regions of EB1b and EB1c were swapped, were fused to the C-terminus of GFP and produced transiently in epidermal cells of onion (*Allium cepa*; Fig. 3B). Wild-type EB1b and EB1c with the EB1b tail (EB1c-Tb) were excluded from the nucleus. Whereas the GFP-EB1b fusion labeled cortical MTs (data not shown), GFP-EB1c-Tb was distributed in the cytoplasm without MT association, indicating that the MT association is impaired by the GFP fusion to the N-terminus of EB1c (also see later). By contrast, wild-type EB1c and the EB1b with the EB1c tail (EB1b-Tc) were both strongly concentrated in the nucleus (Fig. 3B).

By searching for classical NLSs in the EB1c tail, we found a composite motif that was conserved in the EB1c homologs in other plants and consisted of two short basic regions, Box1 and Box2, separated by 17 amino acids (Fig. 3A; supplementary material Fig. S1). This motif with short stretches of basic amino acids was

reminiscent of an NLS, but did not conform to previously reported NLS sequences (Kosugi et al., 2009). We exchanged KRK in Box1 with AAA (m1) and RQR in Box2 with AQA (m2) and transiently produced the wild-type and mutated EB1c tails as C-terminal fusion proteins to the chimeric GFP-β-glucuronidase (GFP-GUS) protein in epidermal cells of onion (Fig. 3B,C). GFP-GUS-Tc^{wt} was efficiently transported into the nucleus, but other chimeric proteins (GFP-GUS, GFP-GUS-Tc^{m1}, GFP-GUS-Tc^{m2} and GFP-GUS-Tc^{m1,m2}) were excluded from the nucleus. These results demonstrate that the basic amino acids in Box1 and Box2 are necessary and that the tail region is sufficient for the nuclear localization of EB1c.

EB1c is required for positioning of spindle poles and chromosome segregation

Because previously reported *eb1* mutants of *Arabidopsis* contained T-DNA insertions in the introns, these mutants might not represent null alleles (Bisgrove et al., 2008). The *eb1a* and *eb1c* alleles used in our study (*eb1a-2* and *eb1c-2*), however, had T-DNA insertions in the exons and did not express full-length transcripts, whereas our *eb1b* allele (*eb1b-3*) had a premature stop codon in the CH domain (Fig. 4A; supplementary material Fig. S5); thus, our mutants were probably null alleles. Growth and morphology of these *eb1* single mutants, *eb1a eb1b* double mutants, and *eb1a eb1b eb1c* triple mutant were indistinguishable from those of the wild type (Fig. 4B,C). No leftward skewing of the mutant roots was observed on the vertical or inclined hard-agar plates, in contrast to previous data (Bisgrove et al., 2008). Different genetic backgrounds of the mutants (Wassilewskija versus Columbia in this study) might underlie this discrepancy. Addition of oryzalin, a MT-destabilizing agent, to the growth medium inhibited root growth of *eb1c-2* more strongly than that of wild-type, *eb1a-2*, *eb1b-3* and the *eb1a eb1b* double mutant (Fig. 4B,C). The effect of oryzalin on triple mutant roots was stronger than that on *eb1c-2* roots, indicating some functional redundancy among the three EB1 members. Meristematic cells of oryzalin-treated *eb1c-2* roots contained recently divided cells in which cell plates were formed at aberrant angles, deviating considerably from the transverse orientation of the cell files (Fig. 4D).

To examine structure and orientation of mitotic MTs, we crossed a GFP-tubulin marker line to *eb1* mutants. The triple mutant was not analyzed because the GFP fluorescence was scarcely detectable in its background. Before breakdown of the nuclear envelope, the preprophase band (PPB) was positioned strictly perpendicular relative to the long axis of the cell in wild-type and *eb1* mutant cells (40 PPB structures were examined for each genotype). Collapsed spindles that did not align at opposing poles (Fig. 5A; supplementary material Movies 4 and 5) were found at an increased frequency in *eb1a eb1b* and even more frequently in *eb1c-2* cells (Fig. 5B) and increased further when seedling roots were grown in the presence of 100 nM oryzalin (Fig. 5B). Measurements of the distance between two poles of noncollapsed spindles revealed that, although oryzalin treatment reduced the pole-to-pole distance in all cell types examined, it was significantly shorter in *eb1c* spindles than that in spindles of the control and the double mutant, both in the presence and absence of the drug (Fig. 5C). The interpolar axis of spindles was mostly positioned longitudinally to the cell file in the control and *eb1a-2 eb1b-3* cells, but more than 50% of the *eb1c-2* spindles were skewed from the longitudinal orientation at angles greater than 10° (Fig. 5D). In the presence of 100 nM oryzalin, the percentages of longitudinally positioned spindles decreased to approximately 60% in the control and *eb1a eb1b* cells and
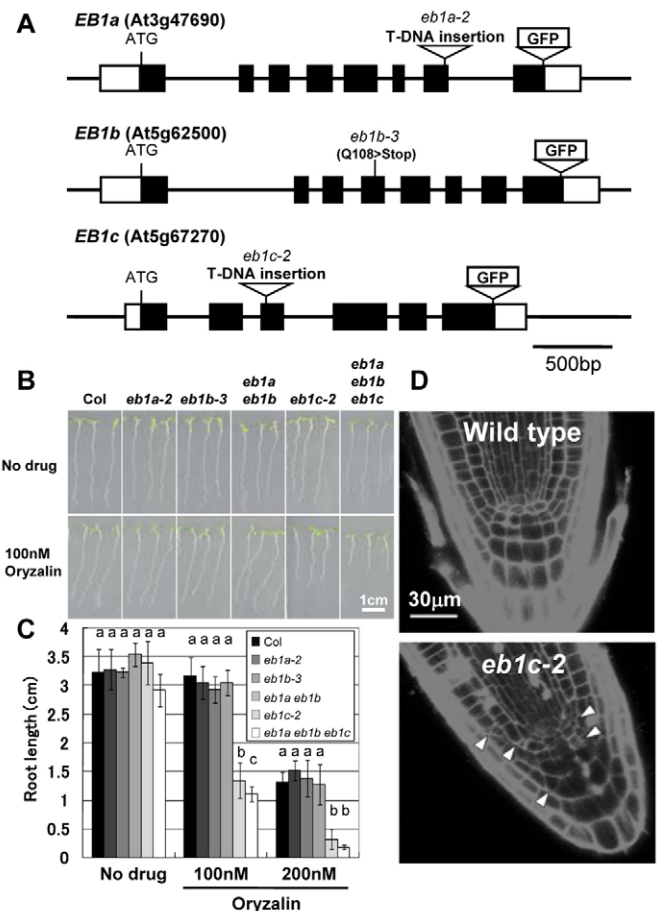

Fig. 4. Phenotypes of *eb1* mutant plants. Seedling roots of the multiple mutants of *eb1a-2*, *eb1b-3*, *eb1c-2* were analyzed. (**A**) Structure of *Arabidopsis EB1* genes. *EB1a* and *EB1b* consist of eight exons (thick bars), whereas *EB1c* has six exons. The protein-coding regions are in black and the 5′- and 3′-untranslated regions in white. The GFP reporters were inserted just before the stop codons. T-DNA insertion sites in *eb1a* and *eb1c* and a mutation site in *eb1b* are indicated. (**B**) Four- to 6-day-old seedlings grown on vertically placed plates, in the presence or absence of 100 nM oryzalin. (**C**) Root growth of 7-day-old seedlings. The data are means (± s.d.) of more than 30 seedlings. Significant differences (*P*<0.01; indicated by different letters) among wild type and *eb1* mutants were determined for each growth condition by one-way ANOVA followed by a Tukey-Kramer test. (**D**) Median longitudinal sections of the root tips of wild-type and *eb1c-2* seedlings grown in the presence of 100 nM oryzalin for 7 days. Arrowheads indicate abnormally oriented cell plates in *eb1c* roots.

approximately 50% in the *eb1c-2* cells. Both without and with oryzalin treatment, the orientations of the *eb1c-2* spindles were statistically differently from those of the control and *eb1a eb1b* spindles (*P*<0.01, a Kruskal-Wallis test followed by a Scheffe's *F* test). Subsequently, some of the tilted spindles rotated and formed phragmoplasts that localized largely transversely to the long axis of the cells (supplementary material Movie 6).

Analysis of the phenotypes of the phragmoplast MT arrays during telophase revealed collapsed phragmoplasts (Fig. 6A) apparently at a higher frequency in the *eb1c-2* cells (approximately 6% of all phragmoplasts) than that in the control (approximately 2%) and *eb1a eb1b* cells (approximately 3%; Fig. 6B). Oryzalin treatment increased the frequency of collapsed phragmoplasts considerably in *eb1c-2* cells (approximately 15%), but the effect of the drug was very moderate
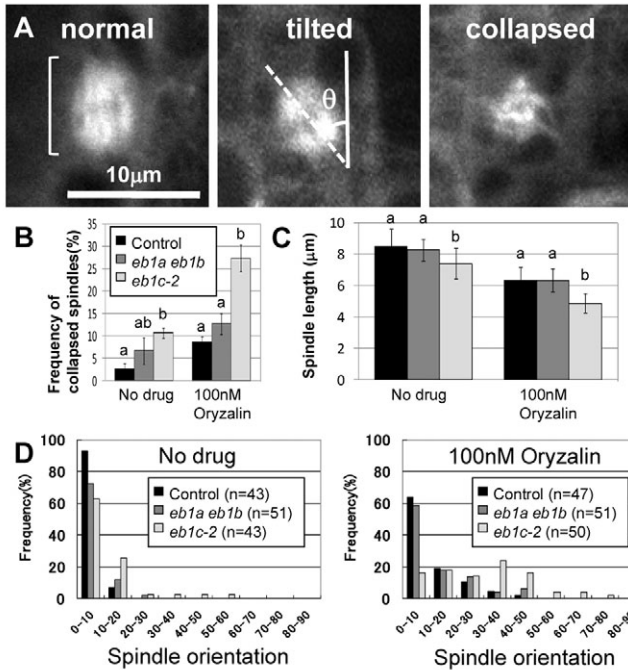
Fig. 5. Spindle characteristics. (**A**) Classification of mitotic spindle structures. (**B**) Frequency of collapsed spindles in dividing control, *eb1a-2*, *eb1b-3* and *eb1c-2* root cells. Fifty spindles were analyzed for each genotype in one treatment of one experiment; the experiments were repeated three times. Significant differences (*P*<0.01; indicated by different letters) among genotypes were determined for each condition by one-way ANOVA followed by a Tukey-Kramer test. (**C**) Spindle length measurements as shown by the bracket in A. Significant differences (*P*<0.01) among genotypes were determined for each condition (*n*=45 for each genotype) by one-way ANOVA followed by a Tukey-Kramer test and indicated by different letters. (**D**) Distribution of the orientation of mitotic spindles. The orientation parallel to the long axis of the cell was designated as 0°, as shown in A.

Fig. 6. Phragmoplast characteristics. (**A**) Classification of phragmoplast structures at the late stage. (**B**) Frequency of collapsed phragmoplasts of dividing control, *eb1a-2*, *eb1b-3*, and *eb1c-2* root cells. Fifty phragmoplasts were analyzed for each genotype in one treatment of one experiment, and the experiments were repeated three times. Significant differences (*P*<0.01; indicated by different letters) among genotypes were determined for each condition by one-way ANOVA followed by a Tukey-Kramer test. (**C**) Phragmoplast width measurements, as indicated by the bracket in A. Significant differences (*P*<0.01; indicated by different letters) among genotypes were determined for each condition (*n*=45 for each genotype) by one-way ANOVA followed by a Tukey-Kramer test. (**D**) Distribution of the orientations of phragmoplasts. The transverse orientation perpendicular to the long axis of the cell was designated as 0°, as shown in A.

in the control and double mutant cells (Fig. 6B). The width of the phragmoplasts was slightly, but significantly, shorter in the *eb1c-2* cells than in the control and *eb1a eb1b* cells, both in the absence and presence of oryzalin (Fig. 6C). During centrifugal outgrowth of the phragmoplasts, skewed phragmoplasts frequently rotated toward the transverse orientation of the cell to the former positions of the PPB. The phragmoplast reorientation compromised the apparently defective spindle positioning; thus, the aberrant orientation of the cell plates was only visible in the oryzalin-treated *eb1c-2* cells (Fig. 6D; *P*<0.01, a Kruskal-Wallis test followed by a Scheffe's *F* test).

To evaluate chromosome movements during mitosis, we labeled kinetochores by stably expressing a tandem dimer variant of the red fluorescent protein fused to centromeric histone H3 (tdTomato-CenH3) in tobacco (*Nicotiana tabacum*) Bright Yellow-2 (BY-2) cells (Kurihara et al., 2008). In two independent transgenic tobacco cell lines, the expression of the endogenous *EB1c*, but not that of the tobacco *EB1a* and/or *EB1b* subtype gene, was significantly and specifically suppressed by an inducible RNA interference (RNAi) construct after addition of estradiol to the culture medium (Fig. 7A). In the *EB1c*-suppressed tobacco cells, kinetochores were aligned on the spindle equator during metaphase, but with a four- to fivefold higher frequently of lagging chromosomes at anaphase than in the control and estradiol-untreated *EB1c* RNAi cells (Fig. 7B,C). These results indicate that tobacco EB1c is required for chromosome segregation and maintenance of the euploid genome.
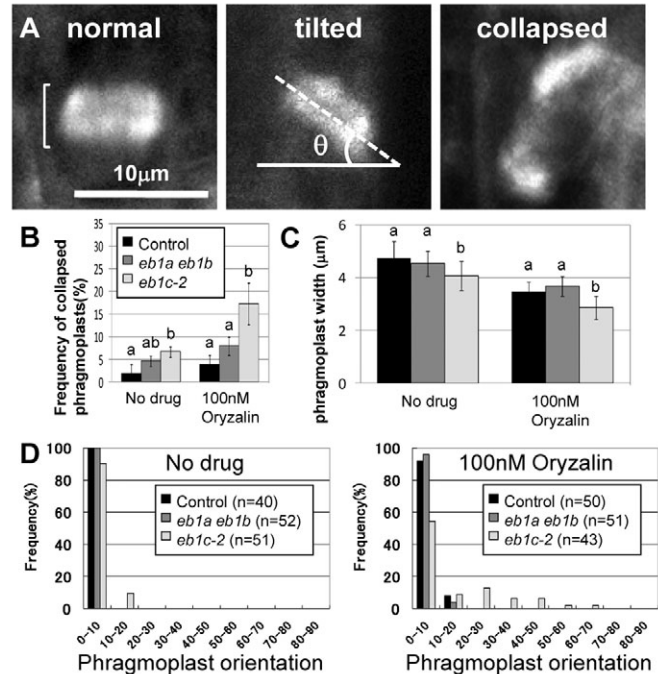
Complementation tests reveal functional specificity of the EB1c tail

To investigate the functional requirement of the EB1c tail, we expressed various *EB1* constructs under the native regulatory elements of *EB1c* in the *eb1c-2* mutant background and scored the root growth of transgenic seedlings in the presence of 100 nM oryzalin (Fig. 8A). Wild-type EB1c efficiently complemented the oryzalin hypersensitivity of *eb1c-2* roots, whereas the EB1c variant, with a defective NLS (EB1c[m1,m2]), only partially restored the root growth. When EB1b was expressed under the *EB1c* promoter, it partially rescued the mutant phenotype. Addition of an artificial NLS to EB1b did not improve the complementation efficiency.

Complementation tests were done with EB1c proteins fused to GFP (Fig. 8A). The N-terminal GFP fusion (GFP-EB1c) was totally ineffective, whereas the C-terminal fusion (EB1c-GFP) completely rescued the mutant phenotype and, thus, was fully functional. GFP-EB1c was not associated with MTs and was evenly distributed in the cytoplasm (Fig. 8B), indicating that the N-terminal GFP fusion inhibited the MT-binding activity. The EB1c lacking the tail region (EB1cΔT-GFP) was capable of tracking the plus end of MTs, but was not targeted to the interphase nucleus in *eb1c-2* (EB1cΔT-GFP was recruited to the nucleus in the wild-type background; supplementary material Fig. S6) and partially complemented the
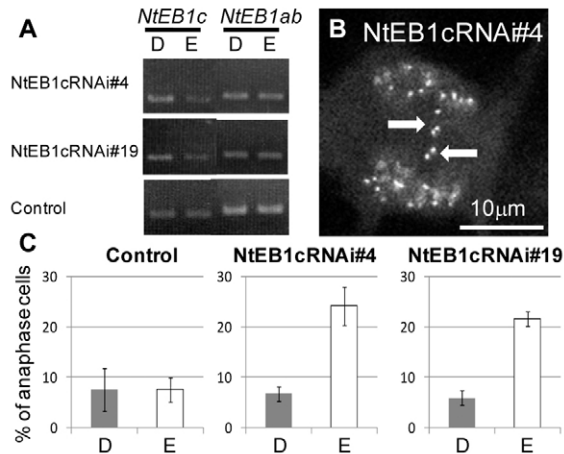
Fig. 7. Analysis of the mitotic outcome in *EB1c*-downregulated tobacco cells. Expression of tobacco (*Nt*) *EB1c* was suppressed after inducing RNAi by estradiol in cultured BY-2 cells. (**A**) RT-PCR expression analysis of *Eb1ab* and *EB1c* in tobacco cells treated with the solvent DMSO (D) or the inducer estradiol (E) for 3 days. The *EB1c* mRNA levels were 74% and 63% lower in the *EB1c* RNAi #4 and #19 lines, respectively, than in the control line. (**B**) An *EB1c* RNAi #4 cell at anaphase after the estradiol treatment, with lagging chromosomes (arrows). Kinetochores were labeled by tdTomato-CenH3. (**C**) Number of anaphase tobacco cells with lagging chromosomes after treatment with DMSO (D) or estradiol (E). Forty anaphase cells were analyzed for each cell line and treatment. Bars represent mean ± s.d.

mutant phenotype. Addition of an artificial NLS effectively targeted the tail-less EB1c (EB1cΔT-GFP-NLS) to the nucleus, but still resulted in a partial rescue. Importantly, the nucleus-targeted EB1c with mutations in its own NLS (EB1c^{m1m2}-GFP-NLS) fully complemented the mutant, indicating that the EB1c tail not only contains a NLS, but also (an) additional functionally important motif(s) absent in EB1b.

Discussion

Functional domains of *Arabidopsis* EB1 proteins

Two prominent structural features of the EB1 family proteins are the N-terminal CH and the C-terminal CC domains that have been shown to be responsible for the interaction with MTs and for dimerization, respectively, in yeast and vertebrates (Akhmanova and Steinmetz, 2008). The CH domain alone associates with MTs, when expressed in human cells (Bu and Su, 2003) and artificially dimerized in vitro (Komarova et al., 2009), and is targeted to growing MT ends when combined with the adjacent linker region (Komarova et al., 2009). The linker region is required for the polymerization-enhancing activity of the CH domain of the yeast EB1 family proteins, Mal3p and Bim1p (des Georges et al., 2008; Zimniak et al., 2009). Our MT-binding assays with various fragments of EB1b and EB1c are consistent with previous data suggesting important functional roles of the linker region. For dimerization of EB1b, the two conserved residues (Y217 and I224) in the first α-helix of the EB1 homologous region were essential, as reported for the human EB1 (Slep et al., 2005), but the CH domain was dispensable. Therefore, the biochemical functions of the structurally homologous EB1 domains are basically conserved in the *Arabidopsis* EB1 proteins.

Another functional region in the EB1 proteins is the flexible acidic tail with the terminal EEY/F motif that is important for self-inhibition and binding to several CAP-Gly-domain-containing
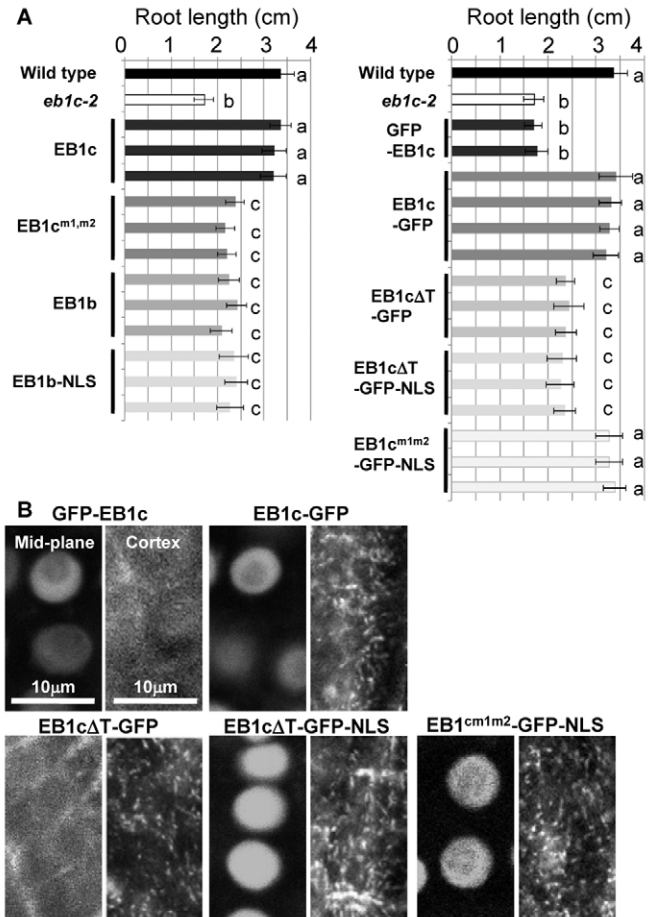

Fig. 8. Complementation of *eb1c* by various EB1 constructs. Transgenes were expressed under the regulatory elements of *Arabidopsis EB1c* in the *eb1c-2* background. (**A**) Root length of 7-day-old seedlings grown in the presence of 100 nM oryzalin. Each bar represents mean root length (± s.d.) of more than 30 seedlings from wild-type, *eb1c* mutant or individual homozygous transgenic lines. Significant differences ($P<0.01$; indicated by different letters) among wild-type, *eb1c*, and transgenic lines were determined by one-way ANOVA followed by a Tukey-Kramer test. (**B**) Nuclear localization of EB1 proteins fused to GFP. Nuclear regions at interphase (left panel of each pair) and the cortical images of the cells just after completion of cytokinesis (right). Comet-like dots were localized at growing plus ends of cortical MTs.

+TIPs, including p150^{glued} and the cytoplasmic linker protein 170 (CLIP170) (Steinmetz and Akhmanova, 2008). Since structural homologs of these +TIPs are absent in the sequenced plant genomes (Bisgrove et al., 2004; Guo et al., 2009), it is of particular interest to see whether the C-terminal tail of plant EB1 proteins has conserved functions similar to those of vertebrates. The tail region of the *Arabidopsis* EB1b, which does not terminate with EEY/F, but is rich in Glu residues, indeed inhibited the MT polymerization activity. Plant +TIPs might interact with the EB1b tail in a manner distinct from those of animals, and potentially regulate the MT-assembly-promoting activity of EB1b in a conceptually similar way to that proposed for the p150^{glued}-EB1 interaction (Hayashi et al., 2005).

By contrast, the tail region of EB1c was not inhibitory in our MT assembly assay, but instead possessed two motifs conserved in the EB1c subtype of various plants that functioned as nuclear

targeting signals. These distinct features of the tail region discriminate *Arabidopsis* EB1c from other known EB1 proteins. Interestingly, the budding yeast EB1 protein Bim1p does not possess the terminal EEY/F motif and does not appear to be regulated by autoinhibition between the CH domain and the extreme C-terminus (Zimniak et al., 2009).

Recently, animal EB1-binding proteins, such as the adenomatous polyposis coli protein and CLIP-associated proteins (CLASPs), which do not contain CAP-Gly domains, were shown to use a short polypeptide motif, Ser-X-Ile-Pro, to localize to the MT tips by interacting with the EB1 homology region of EB1 (Honnappa et al., 2009). *Arabidopsis* CLASP partially accumulates at the plus end of growing MTs (Ambrose et al., 2007; Kirik et al., 2007), but without the Ser-X-Ile-Pro motif. Interaction modes of EB1 and partner +TIPs might be highly divergent between mammals and plants.

EB1c regulates mitotic MTs

In cultured cell suspensions of *Arabidopsis*, EB1a-GFP labeled two polar regions of the nuclear periphery before nuclear envelope breakdown in a PPB-dependent manner (Chan et al., 2005). These premitotic bipolar caps were positioned perpendicularly to the PPB and marked the spindle poles upon nuclear envelope breakdown, suggesting that the PPB is involved in a polarization event that promotes early spindle positioning. In *Arabidopsis eb1c* root cells, the bipolar axis of the spindle was variable at metaphase, despite the PPB formation in the correct orientation, perpendicular to the long axis of the cell. When *EB1c* expression was suppressed in cultured tobacco cells, lagging chromosomes were frequently observed at anaphase. These mitotic phenotypes indicate that EB1c is required to maintain spindle bipolarity during premetaphase and/or metaphase and also for efficient segregation of chromosomes at anaphase. In metazoan cells, depletion of EB1 displaces the spindle from the center of the cell, extensively rotates the spindle axis at metaphase, and generates lagging chromosomes at anaphase (Draviam et al., 2006). As kinetochore-MT attachment was not perturbed in the EB1-depleted animal cells, defects in the plus-end dynamics of spindle MTs might underlie such mitotic phenotypes (Draviam et al., 2006). Reductions in kinetochore-MT turnover at early mitosis caused by depletion of MT-depolymerizing kinesins have recently been shown to induce severe chromosome segregation defects in human cells (Bakhoum et al., 2009), indicating that tight control of dynamic behaviors of spindle MTs is essential for ensuring genome stability in both animal and plant cells.

EB1c is a distinct EB subtype specific to vascular plants

The unique C-terminal tail of *Arabidopsis* EB1c contains two motifs (Box1 and Box2) that function as NLSs. The EB1 proteins with these characteristic motifs (as well as other invariant amino acids) at their C-termini are found in various vascular plants, including the lycophyte *Selaginella moellendorfii* (supplementary material Fig. S1), but only the classical non-EB1c-type proteins are encoded in the sequenced genomes of mosses (e.g. *Physcomitrella patens*), algae, yeasts and animals (data not shown).

EB1c formed homodimers, but no efficient heterodimers with EB1a and EB1b in vitro. The EB1c-GFP protein lacking NLSs was targeted to the nucleus in the wild type, but stayed in the cytoplasm in the *eb1c-2* mutant, suggesting that nuclear targeting of EB1 dimers is conferred dominantly by one dimerizing pair of wild-type EB1c. However, EB1a-GFP and EB1b-GFP were not targeted to the nucleus in wild-type meristematic cells where the intact *EB1c*

was expressed. These results indicate that EB1c does not readily form heterodimers with EB1a and EB1b in vivo. Such a selective dimerization among *Arabidopsis* EB1 members should maintain the functional specificities of EB1c.

When *EB1b* was expressed under the control of the *EB1c* regulatory elements, it did not fully complement the oryzalin-hypersensitive phenotype of *eb1c-2* roots, indicating that EB1c is more efficient than EB1b in regulating spindle functions. Accumulation of EB1c in the premitotic nucleus might facilitate the immediate interaction of EB1c on the spindle MTs after disintegration of the nuclear envelope. However, recruitment of either EB1b or C-tail-less EB1c into the interphase nucleus by addition of an artificial NLS did not result in full complementation, hinting at the presence of EB1c-specific function(s) other than NLS. Besides Box1 and Box2, EB1c homologs from various plants share limited numbers of amino acid residues (including a GSPL motif) in their C-terminal tails (supplementary material Fig. S1). Future studies will be directed to analyzing these conserved regions in the EB1c tail, and to identifying plant proteins that associate with the acidic C-terminal tail of the non-EB1c-type EB1 proteins.

Materials and Methods

Production of recombinant EB1 proteins

Full-length and fragments of EB1 cDNAs were cloned between the *Kpn*I and *Bam*HI sites of a modified pET32b (Novagen) in which the thrombin recognition site had been replaced with the recognition site of PreScission protease, and expressed in the *Escherichia coli* strain BL21 DE3 (Novagen). Mutations of the YI EB1 mutant were introduced by PCR with specific primers. Recombinant proteins were affinity-purified with Ni-Sepharose resin (GE Healthcare), treated with PreScission protease (GE Healthcare) to remove the purification tag, and were subsequently purified using Q-Sepharose resin (GE Healthcare).

Co-sedimentation assay of MTs

Tubulin was purified from porcine brain and used as described previously (Yao et al., 2008). The buffer of the purified EB1 proteins was replaced with PEM buffer (0.1 M PIPES, pH 7.0, 1 mM EGTA, 1 mM $MgCl_2$, 1 mM DTT and 1 mM PMSF) and passed through the PD-10 column (GE Healthcare). Taxol-stabilized MTs and recombinant EB1 proteins were incubated at 37°C for 15 minutes in PEM buffer. The final concentration of tubulin was 9.2 µM for full, ΔCH and ΔT fragments of EB1b, and 2.3 µM for other EB1 fragments. The mixtures were centrifuged at 100,000 *g* for 10 minutes. Proteins in the supernatant and the pellet were separated by 15% or 12.5% SDS-PAGE, and stained with Coomassie brilliant blue.

Turbidity assay for MT assembly

After polymerization of 40 µM tubulin in PEM buffer containing 1 mM GTP for 5 minutes at 37°C, the EB1 protein was added at a final concentration of 20 µM for tubulin and 2 µM for EB1 protein. Subsequent tubulin polymerization was continuously monitored by changes in absorbance at 350 nm by means of an UVmini-1240 spectrophotometer (Shimadzu).

Dimerization assays of EB1 proteins

For the yeast two-hybrid interaction assay with the PROQUEST two-hybrid system (Invitrogen), the *EB1b*-coding sequences of the wild type and the YI mutant were fused to the DNA-binding domain (DNA-BD) in pDEST32 and to the activation domain (AD) in pDEST22 and transformed into the yeast strain MaV203. For the negative control, bait proteins were transformed together with the empty prey vector pEXP-AD502. The activation of the *HIS* reporter gene was tested by spotting the transformants on synthetic defined (SD) plates without histidine.

For gel filtration, the ΔCH EB1b fragments (121-293) of the wild type and the YI mutant were diluted in a running buffer (25 mM Tris, pH 8.0, 200 mM NaCl) to a final concentration of 32 µM. An aliquot (100 µl) was loaded onto a TSK G3000SWXL gel filtration column (TOSOH). The elution was monitored at 280 nm at a flow rate of 0.3 ml/minute. Proteins in the supernatant and the pellet were separated by 12.5% SDS-PAGE and stained with Coomassie brilliant blue.

Heterodimer formation was analyzed by a pull-down assay. After a full-length EB1 protein with a 5×His tag at the N-terminus (10 µM) had been incubated with a ΔCH fragment of EB1a, EB1b or EB1c (10 µM each) for 5 minutes at 37°C, the sample was passed through a Ni-Sepharose-6 Fast Flow column (GE Healthcare) that had been equilibrated with 20 mM Tris-HCl, pH 7.4, 0.15 M NaCl and 1 mM DTT. The column was washed extensively with the same buffer, and then trapped EB1 proteins were eluted with 50 mM Tris-HCl, pH 7.5, 0.5 M NaCl, 0.5 M imidazole, and analyzed by SDS-PAGE as described above.

Subcellular localization assays with particle bombardment

The N-terminal fragments of EB1b (1-264) and EB1c (1-277) were first cloned between the *Bam*HI and *Kpn*I sites of pUC19; then the tail regions of EB1b (265-293) or EB1c (278-329) were inserted between the *Kpn*I and *Sac*I sites. The assembled chimeric EB1 cDNAs were subcloned between the CaMV 35S promoter and GFP in a modified pUC19 plasmid. The Box1 and Box2 motifs of the EB1c tail were mutated by PCR with specific primers. Wild-type and mutant tail regions were cloned in a pUC19-based plasmid that contained the CaMV 35S promoter and a chimeric GFP-GUS sequence. Test constructs were transiently expressed in onion epidermal cells with a particle delivery system (PDS-1000/He; Bio-Rad Japan).

Transgenic *Arabidopsis* plants

The stop codons in the 5-kb genomic regions of *EB1a* and *EB1b* were replaced by *Sma*I sites, and that of the 5-kb genomic *EB1c* gene by a *Nae*I site. The resulting *EB1* genes, including 2 kb of 5′-upstream sequences, were ligated to *GFP* at the introduced restriction sites and cloned into pBIN19, carrying a hygromycin resistance marker. The binary vectors were introduced into the *Agrobacterium tumefaciens* strain MP90 and used to transform *Arabidopsis thaliana* (L.) Heyhn. plants (Columbia ecotype). Various EB1 constructs were generated based on the *EB1c* genomic backbone and were transformed to the *eb1c-2* mutant for complementation assays. The *m1m2* mutations were introduced by PCR with specific primers. A 3-kb genomic region of *EB1b*, including the whole coding region and a 0.9-kb 3′-downstream region was ligated to the 2-kb 5′-upstream sequence of *EB1c*. *GFP-EB1c* was generated by inserting *GFP* (without stop codon) at the translational initiation ATG in the genomic *EB1c* clone. To create *EB1cΔT-GFP*, the C-terminal region (1579-1737 bp) was removed from *EB1c-GFP* by PCR. An artificial NLS (Chiu et al., 1996) was introduced by PCR at the C-termini of EB1b and EB1cΔT-GFP. *Arabidopsis* plants were transformed by the floral dip method (Clough and Bent, 1998). Homozygous plants of the T3 generation were analyzed for all transgenic lines.

Analyses of *Arabidopsis eb1* mutants

T-DNA insertion lines of *eb1a-2* (CS858017) and *eb1c-2* (SALK_018475) were obtained from the Arabidopsis Biological Resource Center (Columbus, OH), whereas the *eb1b-3* mutant was identified by the Seattle TILLING Project (Till et al., 2003). T-DNAs were inserted at 1510 bp and 630 bp downstream from the predicted translation start sites of *EB1a* and *EB1c*, respectively. In *eb1b-3*, a cytosine at 1147 bp was replaced with a thymine, thus creating a premature stop codon instead of Gln108 and an *Mse*I restriction site. These *eb1* mutants (Col-0 background) were crossed to a GFP-TUA6 MT-labeling line (Ueda et al., 1999). Plant growth conditions and oryzalin treatments have been described elsewhere (Naoi and Hashimoto, 2004). Root tips of 7-day-old seedlings were stained with 10 μM propidium iodide. GFP-TUA6-labeled mitotic MTs in dividing root cells were examined with a C1-ECLIPSE E600 confocal laser scanning microscope (Nikon, Tokyo, Japan).

Expression of *EB1a* and *EB1b* was analyzed by RT-PCR. Total RNA was isolated from *Arabidopsis* seedlings with the RNeasy kit (Qiagen). Reverse transcription-PCR was done with SuperScript II reverse transcriptase (Invitrogen) and amplified with Ex Taq DNA polymerase (TaKaRa Bio) under the following conditions: 27 cycles at 94°C for 30 seconds, 55°C for 30 seconds and 72°C for 60 seconds. The PCR primers were 5′-CATGCCATGGCGACGAACATCGGA-3′ and 5′-CCGCTC-GAGTTAGGCTTGAGTCTTTTCTTC-3′ for *AtEB1a*, and 5′-CATGCCATGGCT-ACGAACATTGGG-3′ and 5′-CCGCTCGAGTCAGCAGGTCAAGAGAGGAG-3′ for *AtEB1c*.

The *eb1b* mutation was identified by detecting a polymorphism introduced by the mutation. Genomic DNA was extracted by a standard procedure. An *EB1b* genomic fragment was amplified by PCR with Ex Taq DNA polymerase (TaKaRa Bio) under the following conditions: 30 cycles at 94°C for 30 seconds, 55°C for 30 seconds, and 72°C for 30 seconds. The PCR primers were 5′-ATCTCCCACTTTT-TAGGGTAACTTT-3′ and 5′-GTTCTTGGATTCAAAGTTGAGAGAA-3′. After digestion with *Mse*I, PCR products were analyzed by electrophoresis on agarose gels.

Suppression of tobacco *EB1c* gene in cultured BY-2 cells

The plasmid expressing tdTomato-CenH3 (Kurihara et al., 2008) was modified to contain the neomycin phosphotransferase II (*NPTII*)-encoding gene and used to establish a kanamycin-resistant kinetochore marker line of cultured tobacco BY-2 cells with *Agrobacterium tumefaciens* strain EHA105 and a transformation protocol (http://www.plantgenetics.rug.ac.be/~dagee). An inducible RNAi cassette containing an inverted repeat of the partial *NtEB1c* cDNA fragment (+769 to +1049) and the *pdk* intron of pHANNIBAL (Wesley et al., 2001) was transferred to a multicloning site downstream of the OLexA promoter in pER8 (Zuo et al., 2000). The pER8-NtEB1cRNAi vector was used to transform the tdTomato-CenH3-expressing BY-2 cells. Hygromycin-resistant calli were transferred to a liquid medium to establish suspension cultures. Two-day-old tobacco BY-2 cells were treated with 2 μM β-estradiol or dimethylsulfoxide (DMSO) alone. After 3 days, cells in anaphase were examined for lagging chromosomes. DNA sequences of *NtEB1ab* and *NtEB1c* were deposited in NCBI (accession numbers AB500051 and AB500051, respectively).

RNA extraction and RT-PCR were done as described above, but under the following conditions: 23 cycles at 94°C for 30 seconds, 55°C for 30 seconds and seconds 72°C

for 30 seconds. The PCR primers were 5′-CAGTGTCCAGAGATTGAAAACCTCC-3′ and 5′-ACCCAGAGAGAACAAGTCAT-3′ for *NtEB1c* and 5′-TGGGAAG-GAACGAAATGTGAAGGG-3′ and 5′-TCTGCCAATGCTGATTCTCTTGCA-3′ for *NtEB1ab*.

Quantitative RT-PCR

RNA was extracted from different anatomical parts of *Arabidopsis* seedlings with the RNeasy kit (Qiagen). cDNA was prepared from 1 μg of total RNA with Suprescript III reverse transcriptase (Invitrogen). The amount of target RNAs was quantified by an iCycler apparatus (Bio-Rad) with the Platinum SYBR Green qPCR Supermix-UDG kit (Invitrogen) according to the manufacturer's recommendations. PCRs were run in 96-well optical reaction plates heated for 10 minutes at 95°C to activate hot start Taq DNA polymerase, followed by 40 cycles of denaturation for 60 seconds at 95°C, and annealing extension for 60 seconds at 58°C. Targets were quantified with specific primer pairs designed with the Beacon Designer 4.0 (Premier Biosoft International). All PCRs were done in triplicate. The primers used to quantify the expression levels were: 5′-CAAGCTCCGGGATGTAGAGGA-3′ and 5′-TTGCAT-ACAGTATCTTCTTCACTGC-3′ for *EB1a*, 5′-TCCTGTGGCTACTTCCAACA-3′ and 5′-TGCACTTCGGCTGATGAGT-3′ for *EB1b*, and 5′-CAAAACCCAG-ACACAGAGCA-3′ and 5′-CTGCTGCTCCAACGTCTTCT-3′ for *EB1c*. The expression levels were normalized to those of *EEF* and *CDKA*. The resulting data were analyzed with qBase v1.3.4 (Hellemans et al., 2007).

Supplementary material available online at
http://jcs.biologists.org/cgi/content/full/123/3/451/DC1

References

Akhmanova, A. and Steinmetz, M. O. (2008). Tracking the ends: a dynamic protein network controls the fate of microtubule tips. *Nat. Rev. Mol. Cell. Biol.* **9**, 309-322.

Ambrose, J. C., Shoji, T., Kotzer, A. M., Pighin, J. A. and Wasteneys, G. O. (2007). The *Arabidopsis CLASP* gene encodes a microtubule-associated protein involved in cell expansion and division. *Plant Cell* **19**, 2763-2775.

Bakhoum, S. F., Thompson, S. L., Manning, A. L. and Compton, D. A. (2009). Genome stability is ensured by temporal control of kinetochore-microtubule dynamics. *Nat. Cell Biol.* **11**, 27-35.

Bieling, P., Laan, L., Schek, H., Munteanu, E. L., Sandblad, L., Dogterom, M., Brunner, D. and Surrey, T. (2007). Reconstitution of a microtubule plus-end tracking system *in vitro*. *Nature* **450**, 1100-1105.

Bieling, P., Kandels-Lewis, S., Telley, I. A., van Dijk, J., Janke, C. and Surrey, T. (2008). CLIP-170 tracks growing microtubule ends by dynamically recognizing composite EB1/tubulin-binding sites. *J. Cell Biol.* **183**, 1223-1233.

Bisgrove, S. R., Hable, W. E. and Kropf, D. L. (2004). +TIPs and microtubule regulation. The beginning of the plus end in plants. *Plant Physiol.* **136**, 3855-3863.

Bisgrove, S. R., Lee, Y.-R. J., Liu, B., Peters, N. T. and Kropf, D. L. (2008). The microtubule plus-end binding protein EB1 functions in root responses to touch and gravity signals in *Arabidopsis*. *Plant Cell* **20**, 396-410.

Bu, W. and Su, L.-K. (2003). Characterization of functional domains of human EB1 family proteins. *J. Biol. Chem.* **278**, 49721-49731.

Chan, J., Calder, G. M., Doonan, J. H. and Lloyd, C. W. (2003). EB1 reveals mobile microtubule nucleation sites in *Arabidopsis*. *Nat. Cell Biol.* **5**, 967-971.

Chan, J., Calder, G., Fox, S. and Lloyd, C. (2005). Localization of the microtubule end binding protein EB1 reveals alternative pathways of spindle development in Arabidopsis suspension cells. *Plant Cell* **17**, 1737-1748.

Chiu, W.-l., Niwa, Y., Zeng, W., Hirano, T., Kobayashi, H. and Sheen, J. (1996). Engineered GFP as a vital reporter in plants. *Curr. Biol.* **6**, 325-330.

Clough, S. J. and Bent, A. F. (1998). Floral dip: a simplified method for *Agrobacterium*-mediated transformation of *Arabidopsis thaliana*. *Plant J.* **16**, 735-743.

des Georges, A., Katsuki, M., Drummond, D. R., Osei, M., Cross, R. A. and Amos, L. A. (2008). Mal3, the *Schizosaccharomyces pombe* homolog of EB1, changes the microtubule lattice. *Nat. Struct. Mol. Biol.* **15**, 1102-1108.

Dixit, R., Chang, E. and Cyr, R. (2006). Establishment of polarity during organization of the acentrosomal plant cortical microtubule array. *Mol. Biol. Cell* **17**, 1298-1305.

Draviam, V. M., Shapiro, I., Aldridge, B. and Sorger, P. K. (2006). Misorientation and reduced stretching of aligned sister kinetochores promote chromosome missegregation in EB1- or APC-depleted cells. *EMBO J.* **25**, 2814-2827.

Green, R. A., Wollman, R. and Kaplan, K. B. (2005). APC and EB1 function together in mitosis to regulate spindle dynamics and chromosome alignment. *Mol. Biol. Cell* **16**, 4609-4922.

Guo, L., Ho, C.-M. K., Kong, Z., Lee, Y.-R. J., Qian, Q. and Liu, B. (2009). Evaluating the microtubule cytoskeleton and its interacting proteins in monocots by mining the rice genome. *Ann. Bot.* **103**, 387-402.

Hayashi, I., Wilde, A., Mal, T. K. and Ikura, M. (2005). Structural basis for the activation of microtubule assembly by the EB1 and p150^Glued complex. *Mol. Cell* **19**, 449-460.

Hellemans, J., Mortier, G., De Paepe, A., Speleman, F. and Vandesompele, J. (2007). qBase relative quantification framework and software for management and automated analysis of real-time quantitative PCR data. *Genome Biol.* **8**, R19.

Honnappa, S., Montenegro Gouveia, S., Weisbrich, A., Damberger, F. F., Bhavesh, N. S., Jawhari, H., Grigoriev, I., van Rijssel, F. J. A., Buey, R. M., Lawera, A. et al. (2009). An EB1-binding motif acts as a microtubule tip localization signal. *Cell* **138**, 366-376.

Ishida, T., Thitamadee, S. and Hashimoto, T. (2007). Twisted growth and organization of cortical microtubules. *J. Plant Res.* **120**, 61-70.

Kirik, V., Herrmann, U., Parupalli, C., Sedbrook, J. C., Ehrhardt, D. W. and Hűlskamp, M. (2007). CLASP localizes in two discrete patterns on cortical microtubules and is required for cell morphogenesis and cell division in *Arabidopsis*. *J. Cell Sci.* **120**, 4416-4425.

Komarova, Y., De Groot, C. O., Grigoriev, I., Montenegro Gouveia, S., Munteanu, E. L., Schober, J. M., Honnappa, S., Buey, R. M., Hoogenraad, C. C., Dogterom, M. et al. (2009). Mammalian end binding proteins control persistent microtubule growth. *J. Cell Biol.* **184**, 691-706.

Kosugi, S., Hasebe, M., Matsumura, N., Takashima, H., Miyamoto-Sato, E., Tomita, M. and Yanagawa, H. (2009). Six classes of nuclear localization signals specific to different binding grooves of importin α. *J. Biol. Chem.* **284**, 478-485.

Kurihara, D., Matsunaga, S., Uchiyama, S. and Fukui, K. (2008). Live cell imaging reveals plant aurora kinase has dual roles during mitosis. *Plant Cell Physiol.* **49**, 1256-1261.

Manna, T., Honnappa, S., Steinmetz, M. O. and Wilson, L. (2008). Suppression of microtubule dynamic instability by the +TIP protein EB1 and its modulation by the CAP-Gly domain of p150^Glued. *Biochemistry* **47**, 779-786.

Mathur, J., Mathur, N., Kernebeck, B., Srinivas, B. P. and Hülskamp, M. (2003). A novel localization pattern for an EB1-like protein links microtubule dynamics to endomembrane organization. *Curr. Biol.* **13**, 1991-1997.

Naoi, K. and Hashimoto, T. (2004). A semidominant mutation in an Arabidopsis mitogen-activated protein kinase phosphatase-like gene compromises cortical microtubule organization. *Plant Cell* **16**, 1841-1853.

Slep, K. C., Rogers, S. L., Elliott, S. L., Ohkura, H., Kolodziej, P. A. and Vale, R. D. (2005). Structural determinants for EB1-mediated recruitment of APC and spectraplakins to the microtubule plus end. *J. Cell Biol.* **168**, 587-598.

Steinmetz, M. O. and Akhmanova, A. (2008). Capturing protein tails by CAP-Gly domains. *Trends Biochem. Sci.* **33**, 535-545.

Till, B. J., Reynolds, S. H., Greene, E. A., Codomo, C. A., Enns, L. C., Johnson, J. E., Burtner, C., Odden, A. R., Young, K., Taylor, N. E. et al. (2003). Large-scale discovery of induced point mutations with high-throughput TILLING. *Genome Res.* **13**, 524-530.

Tirnauer, J. S. and Bierer, B. E. (2000). EB1 proteins regulate microtubule dynamics, cell polarity, and chromosome stability. *J. Cell Biol.* **149**, 761-766.

Tirnauer, J. S., Canman, J. C., Salmon, E. D. and Mitchison, T. J. (2002). EB1 targets to kinetochores with attached, polymerizing microtubules. *Mol. Biol. Cell* **13**, 4308-4316.

Ueda, K., Matsuyama, T. and Hashimoto, T. (1999). Visualization of microtubules in living cells of transgenic *Arabidopsis thaliana*. *Protoplasma* **206**, 201-206.

Vitre, B., Coquelle, F. M., Heichette, C., Garnier, C., Chrétien, D. and Arnal, I. (2008). EB1 regulates microtubule dynamics and tubulin sheet closure *in vitro*. *Nat. Cell Biol.* **10**, 415-421.

Wesley, S. V., Helliwell, C. A., Smith, N. A., Wang, M. B., Rouse, D. T., Liu, Q., Gooding, P. S., Singh, S. P., Abbott, D., Stoutjesdijk, P. A. et al. (2001). Construct design for efficient, effective and high-throughput gene silencing in plants. *Plant J.* **27**, 581-590.

Yao, M., Wakamatsu, Y., Itoh, T. J., Shoji, T. and Hashimoto, T. (2008). *Arabidopsis* SPIRAL2 promotes uninterrupted microtubule growth by suppressing the pause state of microtubule dynamics. *J. Cell Sci.* **121**, 2372-2381.

Zimmermann, P., Hirsch-Hoffmann, M., Hennig, L. and Gruissem, W. (2004). GENEVESTIGATOR. Arabidopsis microarray database and analysis toolbox. *Plant Physiol.* **136**, 2621-2632.

Zimniak, T., Stengl, K., Mechtler, K. and Westermann, S. (2009). Phosphoregulation of the budding yeast EB1 homologue Bim1p by Aurora/lpl1p. *J. Cell Biol.* **186**, 379-391.

Zuo, J., Niu, Q.-W. and Chua, N.-H. (2000). An estrogen receptor-based transactivator XVE mediates highly inducible gene expression in transgenic plants. *Plant J.* **24**, 265-273.